A&A, 689, A89 (2024)
https://doi.org/10.1051/0004-6361/202449290

Astronomy & Astrophysics

The true nature of HE 0057-5959, the most metal-poor, Li-rich star

A. Mucciarelli[1,2,*], P. Bonifacio[3], L. Monaco[4], M. Salaris[5,6], and M. Matteuzzi[1,2]

[1] Dipartimento di Fisica e Astronomia "Augusto Righi", Alma Mater Studiorum, Universitá di Bologna, Via Gobetti 93/2, 40129 Bologna, Italy
[2] INAF – Osservatorio di Astrofisica e Scienza dello Spazio di Bologna, Via Gobetti 93/3, 40129 Bologna, Italy
[3] GEPI, Observatoire de Paris, Université PSL, CNRS, 5 Place Jules Janssen, 92190 Meudon, France
[4] Universidad Andres Bello, Facultad de Ciencias Exactas, Departamento de Ciencias Físicas - Instituto de Astrofísica, Autopista Concepcion-Talcahuano 7100, Talcahuano, Chile
[5] Astrophysics Research Institute, Liverpool John Moores University, 146 Brownlow Hill, Liverpool L3 5RF, UK
[6] INAF – Osservatorio Astronomico d'Abruzzo, via M. Maggini, 64100 Teramo, Italy

Received 19 January 2024 / Accepted 24 June 2024

ABSTRACT

The Li-rich stars are a class of rare objects with a surface lithium abundance, A(Li), that exceeds that of other stars in the same evolutionary stage. The origin of these stars is still debated, and valuable routes to look at include the Cameron-Fowler mechanism, a mass-transfer process in a binary system, or the engulfment of rocky planets or brown dwarfs. Metal-poor ([Fe/H]<−1 dex) stars are only a small fraction of the entire population of Li-rich stars. We observed the metal-poor ([Fe/H]=−3.95±0.11 dex) giant star HE 0057-5959 with MIKE at the Magellan Telescope, deriving $A(Li)_{NLTE}$=+2.09±0.07 dex. Such an Li abundance is significantly higher, by about 1 dex, than that of other stars at the same evolutionary stage. A previous analysis of the same target suggested that its high A(Li) reflects an ongoing first-dredge-up process. We revised the nature of HE 0057-5959 by comparing its stellar parameters and A(Li) with appropriate stellar evolution models describing Li depletion due to the deepening of the convective envelope. This comparison rules out that HE 0057-5959 is caught during its first dredge-up, the latter having already ended according to the parameters of this star. Its A(Li), remarkably higher than the typical lithium plateau drawn by similar giant stars, demonstrates that HE 0057-5959 joins the class of the rare metal-poor, Li-rich stars. HE 0057-5959 is the most metal-poor, Li-rich star discovered so far. We considered different scenarios to explain this star also comparing it with the other metal-poor, Li-rich stars. No internal mixing able to activate the Cameron-Fowler mechanism is known for metal-poor stars at this evolutionary stage. The engulfment of planets is also disfavoured because such metal-poor stars should not host planets. Finally, HE 0057-5959 is one of the most Na-rich among the Li-rich stars, and we found that a strong excess of Na abundance is common to all three Li-rich stars with [Fe/H]<−3 dex. This finding could support the scenario of mass transfer from a massive companion star (able to simultaneously produce large amounts of both elements) in a binary system, even if we found no evidence of radial velocity variations.

Key words. stars: abundances – stars: atmospheres

1. Introduction

Lithium (Li) is one of the few nuclei produced during the Big Bang nucleosynthesis. Because of their fragility, the Li nuclei are immediately destroyed in stellar layers exceeding temperatures of $\sim 2.5 \times 10^6$ K. In a low-mass star, the surface Li abundance A(Li) changes with time, and its changes reflect the main episodes of mixing occurring during the evolution of the star. When the convective envelope deepens into the stellar interior reaching stellar layers hot enough to burn Li, Li-free material is brought to the surface reducing A(Li). The evolution of A(Li) with the luminosity (or the gravity) can be described as two phases with constant A(Li), namely the Spite Plateau (Spite & Spite 1982; Bonifacio & Molaro 1997; Aoki et al. 2009) and the lower red giant branch (RGB) plateau (Mucciarelli et al. 2012, 2022), both followed by an abrupt drop corresponding to the first dredge-up (FDU) and the RGB-bump (RGBb) mixing episode, respectively. The A(Li) depletion at the FDU is a natural consequence of the standard stellar evolution (Iben 1967), while to explain the second drop at the RGBb, non-canonical mixing processes have to be included, the most popular one being the thermohaline mixing (see e.g. Charbonnel et al. 2020).

Within this framework, the so-called Li-rich stars are a class of peculiar and rare objects whose A(Li) significantly exceeds that measured in stars of a similar evolutionary stage. In some cases (see e.g. Koch et al. 2011; Kowkabany et al. 2022), metal-poor stars have an A(Li) higher than the abundance formed during the Big Bang and inferred by the baryon density obtained from the Wilkinson Microwave Anisotropy Probe (WMAP) and Planck satellites (A(Li)=+2.72±0.04 dex, Coc & Vangioni 2017), while some metal-rich stars have an A(Li) higher than that of the interstellar medium (A(Li)∼+3.3 dex; Asplund et al. 2009). These very high A(Li) values suggest that Li is not preserved, and other production mechanisms must be at work. Their frequency is ∼1% or less of all the stars (Kirby et al. 2016; Casey et al. 2016; Gao et al. 2019; Deepak et al. 2020). They have been observed at all metallicity (Ruchti et al. 2011; Martell & Shetrone 2013; Gao et al. 2019; Sitnova et al. 2023), at all evolutionary stages (Kirby et al. 2016; Li et al. 2018), in the Milky Way halo (Ruchti et al. 2011; Li et al. 2018), the thick disc (Monaco et al. 2011), the thin disc (Casey et al. 2016; Deepak et al. 2020), the bulge (Gonzalez et al. 2009), dwarf spheroidal galaxies (Kirby et al. 2012), globular clusters (GCs, Smith et al. 1999; Ruchti et al. 2011; Koch et al. 2011; Monaco et al. 2012; D'Orazi et al. 2015; Kirby et al. 2016;

*Corresponding author; alessio.mucciarelli2@unibo.it

Mucciarelli et al. 2019; Sanna et al. 2020), and in open clusters (Monaco et al. 2014).

Li-rich stars could be explained as invoking different classes of processes, namely the internal production or external origin of the extra Li. Three main groups of processes have been proposed to explain the existence of these stars, namely the Cameron-Fowler mechanism, mass transfer in binary systems, and the engulfment of small bodies. These are listed in the following paragraphs.

(a) The Cameron-Fowler mechanism – Cameron (1955) and Cameron & Fowler (1971) proposed a mechanism to produce fresh Li in asymptotic giant branch (AGB) stars experiencing the hot bottom burning. ^{7}Li is produced after the decay of ^{7}Be. However, the temperatures needed to produce ^{7}Be from α-capture on ^{3}He are one order of magnitude higher than the temperature of Li burning. Therefore, new Li is immediately destroyed, but if ^{7}Be is fast transported towards cooler regions, Li can survive. The Cameron-Fowler mechanism, originally proposed for intermediate-mass AGB stars (indicatively in the mass range 4–8 $M_{\odot}$, see e.g. Sackmann & Boothroyd 1992; Ventura & D'Antona 2011), can work whenever a mechanism carries ^{7}Be to cooler stellar regions. In the case of AGB stars, this process is driven by the convection, being the bottom of the convective envelope hot enough to produce ^{7}Be. The existence of Li-rich stars at different metallicity, mass and evolutionary stage can be explained with the Cameron-Fowler mechanism only invoking extra mixing, i.e. thermohaline mixing (Charbonnel & Primas 2005), magneto-thermohaline (Denissenkov et al. 2009), mass-loss mechanisms occurring in RGB (de La Reza et al. 1996). An additional mechanism able to trigger the Cameron-Fowler mechanism is the ingestion of sub-stellar companions, like rocky planets or brown dwarfs causing an increase of angular momentum and a rotationally induced mixing (Denissenkov & Herwig 2004).

(b) Mass transfer processes – the accretion of matter from a companion with an enhancement of Li; for instance, any star able to trigger the Cameron-Fowler mechanism. Intermediate-mass AGB stars are the natural candidates, assuming that the low-mass Li-rich star belongs to a binary system with a massive companion (now evolved as a white dwarf). Possible additional signatures of this process could be an enhancement of those elements produced in the interiors of AGB stars (i.e. carbon and slow neutron-capture elements) and radial-velocity variability.

(c) Planets engulfment – the engulfment of sub-stellar companions, such as rocky planets, hot Jupiters, and brown dwarfs, which have high Li enhancement (Siess & Livio 1999). This process should be coupled with infrared excess, possible strong magnetic fields, and X-ray activities.

In this paper, we discuss the metal-poor giant star HE 0057-5959 (*Gaia* EDR3 4903905598859396480), whose A(Li) has previously been derived by Jacobson et al. (2015) and interpreted as a normal giant star caught during its ongoing FDU.

2. MIKE Observations and chemical analysis

2.1. Observations and radial velocity

The target star HE 0057-5959 was observed with the Magellan Ianmori Kyocera Echelle (MIKE) spectrograph (Bernstein et al. 2003) mounted at the Magellan II Telescope at Las Campanas Observatory, under the programme CN2017B-54 (PI: Monaco) during the night of 27 October 2017. We adopted a 0.7″×5.0″ slit corresponding to a spectral resolution of 53 000 and 42 000, in the blue and the red arm, respectively, and covering the spectral range between ∼3400 and ∼9400 Å. A total exposure time of three by 3000 s was adopted, providing a signal-to-noise ratio of 80 per pixel around the Li line at 6708 Å. The spectral reduction, including bias-subtraction, flat-fielding, spectral extraction, and wavelength calibration was performed with the dedicated CarPy pipeline (Kelson 2003). The heliocentric radial velocity (RV) was measured through a cross-correlation against a synthetic spectrum as template, obtaining +376.2±0.2 km s^{-1}, which is in agreement with the previous estimates by Norris et al. (2013, +375.3 km s^{-1}), Jacobson et al. (2015, +376.7 km s^{-1}), and Arentsen et al. (2019, +377.90±3.98 and +378.23±1.47 km s^{-1}). No RV values are provided by *Gaia*.

2.2. Atmospheric parameters

The effective temperature ($T_{\rm eff}$) and the surface gravity ($\log -g$) were estimated by the photometry in order to avoid significant biases affecting the spectroscopic determinations of these parameters in metal-poor giant stars (see Mucciarelli & Bonifacio 2020). We adopted magnitudes from the early third data release of the ESA/*Gaia* mission (Gaia Collaboration 2016, 2020) and a colour excess of E(B–V)= 0.017 mag by Schlafly & Finkbeiner (2011). The extinction coefficients of the three *Gaia* bands were derived by adopting the iterative procedure described in Lombardo et al. (2021). Effective temperature was estimated using the $(G_{\rm BP} - G_{\rm RP})_0$–$T_{\rm eff}$ transformation by Mucciarelli et al. (2021a), deriving $T_{\rm eff}$= 5420±80 K, where the uncertainty includes those arising from the photometric colour, the colour excess, and the adopted colour–$T_{\rm eff}$ transformation. We checked that $T_{\rm eff}$ derived from the other two *Gaia* colours, $(G_{\rm BP} - G)_0$ and $(G - G_{\rm RP})_0$, are in excellent agreement with those of $(G_{\rm BP} - G_{\rm RP})_0$, $T_{\rm eff}$=5477, and 5426 K, respectively.

Stellar luminosity ($\log(L/L_{\odot}) = -0.4 \cdot (M_{\rm bol} - M_{\odot})$) was calculated adopting the photogeometric distance posterior from the *Gaia* parallax provided by Bailer-Jones et al. (2021) and the bolometric correction calculated from a new grid of synthetic fluxes (Mucciarelli et al. in prep.) computed with the code `ATLAS9` (Kurucz 2005). The surface gravity ($\log -g$= −10.32 + $\log(M)$ +4·$T_{\rm eff}$− $\log(L)$) was obtained adopting the photometric $T_{\rm eff}$ and the stellar luminosity described above and a stellar mass equal to 0.76 $M_{\odot}$, which is a reasonable value for RGB stars with old ages and low metallicities according to the theoretical isochrones of Pietrinferni et al. (2021). Ages in the range of ∼11–13 Gyr, which is reasonable for a very metal-poor star such as HE 0057-5959, provide very similar stellar masses along the RGB that are lower than ∼0.82 $M_{\odot}$ with a negligible impact (less than 0.04 dex) on $\log -g$. In the quoted $\log -g$ uncertainty we accounted for uncertainties in the $T_{\rm eff}$, luminosity, and adopted stellar mass.

Microturbulent velocity was estimated spectroscopically by minimising any trend between the abundances from Fe I lines and their reduced equivalent widths. The final parameters for HE 0057-5959 are $T_{\rm eff}$ = 5420±80 K, $\log -g$ = 3.05±0.10, $\log(L/L_{\odot})$ = 1.18±0.14, and $v_{\rm t}$= 1.5±0.2 km s^{-1} (see Table 1). These values are in good agreement with those estimated by Jacobson et al. (2015): $T_{\rm eff}$ = 5413 K, $\log -g$ = 3.41, and $v_{\rm t}$ =1.4 km s^{-1}. On the other hand, the temperature provided by Norris et al. (2013) is cooler (5257 K) and derived as the average of temperatures from spectrophotometric flux and Balmer lines. For the chemical analysis of this star, Yong et al. (2013) adopted the $T_{\rm eff}$ of Norris et al. (2013), while a new value of $\log -g$ (2.65 dex) was derived based on the stellar temperature and a theoretical isochrone with an appropriate metallicity and

Table 1. Stellar parameters for target star HE 0057-5959.

Parameter	Value
$T_{\rm eff}$	5420 ± 80 K
log $-g$	3.05 ± 0.10
$v_{\rm t}$	1.5 ± 0.2 km s^{-1}
log($L/L_{\odot}$)	1.18 ± 0.14

age of 10 Gyr. Their lower log $-g$ reflects mainly the difference in $T_{\rm eff}$ between our and their analysis.

2.3. Chemical analysis

Abundances of Mg, Al, Si, Ca, Ti, and Fe were obtained from measured equivalent widths (EWs) using the code GALA (Mucciarelli et al. 2013a), while for atomic transitions affected by blending, isotopic and/or hyperfine splittings (Li, Na, Sr, and Ba) and molecular features (G band for C), the abundances were derived through an χ^2-minimisation between the observed lines and grids of synthetic spectra calculated with SYNTHE (Kurucz 2005). For other species, spectral lines are too weak and undetectable because of the very low metallicity of the target star, coupled with its relatively high $T_{\rm eff}$, also preventing useful upper limits. We also checked the possibility of measuring N and ^{12}C/^{13}C, but we cannot identify ^{13}C transitions or CN molecular bands at 3870-3885 Å. Despite the importance of N and ^{12}C/^{13}C, the derived upper limits are not meaningful ([N/Fe]<+3.5 dex, ^{12}C/^{13}C>5) and they do not provide useful insights for the interpretation of the target star. In this analysis, we adopted an ATLAS9 model atmosphere (Kurucz 1993, 2005) calculated with a new opacity distribution function (Mucciarelli et al. in prep.) with [Fe/H]=–4.0 dex and [α/Fe]=+0.4 dex.

Abundance ratios scaled on the solar abundances by Lodders (2010) and Caffau et al. (2011) are listed in Table 2, together with the number of measured lines and the total uncertainty. The latter was computed by adding the internal error and that arising from the adopted atmospheric parameters in quadrature (uncertainties in the derived parameters are discussed in Sect. 2.2). The internal error is estimated as the standard error of the mean ($\sigma/\sqrt{(N_{\rm lines})}$) when at least two lines are measured. For elements with one only transition, we consider the uncertainty on the abundance as obtained from the EW error or from Monte Carlo simulations; this is for lines measured from EWs and spectral synthesis, respectively (see details in Mucciarelli et al. 2013b). In Table 2 we report both LTE and NLTE abundances, in the latter case adopting the corrections of Wang et al. (2021) for Li, Lind et al. (2011) for Na, Nordlander & Lind (2017) for Al, Bergemann et al. (2013) for Si, and Mashonkina et al. (2023) for the other elements. The atomic data of the measured atomic lines are listed in Appendix B.

We derived [Fe/H]=–3.95±0.11 dex. Departures from LTE increase the Fe abundance of this star by ~+0.22 dex (Mashonkina et al. 2023). In the following discussion, we refer to the LTE [Fe/H] for consistency with the [Fe/H] values derived for all the other Li-rich metal-poor stars known to date, but the use of NLTE [Fe/H] does not change our conclusion on the nature of HE 0057-5959. The star is enhanced in [α/Fe] (Mg, Si, Ca, and Ti) and characterised by sub-solar [Sr/Fe] and [Ba/Fe]. Also, the star is enhanced in [C/Fe] (+1.07 dex), indicating that it can be labelled as CEMP-no (enhanced in C but not in s-process elements), as already suggested by Jacobson et al. (2015). The comparison with the abundances measured by Yong et al. (2013) and Jacobson et al. (2015) is discussed in Appendix C.

Table 2. LTE and NLTE chemical abundances measured in HE 0057-5959, together with the number of used lines and the total uncertainty.

Ion	$N_{\rm lines}$	LTE	NLTE	σ
		(dex)	(dex)	(dex)
A(Li)	1	+2.05	2.09	0.07
[C/Fe]	1	+1.07	–	0.10
[Na/Fe]	2	+1.92	+1.17	0.08
[Mg/Fe]	4	+0.54	+0.41	0.05
[Al/Fe]	2	–0.11	+0.29	0.16
[Si/Fe]	1	+0.85	+0.63	0.15
[Ca/Fe]	1	+0.44	+0.22	0.07
[Ti II/Fe]	3	+0.44	+0.41	0.10
[Fe/H]	21	–3.95	–3.75	0.11
[Sr II/Fe]	1	–1.11	–1.12	0.15
[Ba II/Fe]	1	–1.47	–1.49	0.20

Notes. The abundances are reported as [X/Fe], except for Li (A(Li)) and Fe ([Fe/H]). The NLTE abundance ratios [X/Fe] are calculated assuming the NLTE [Fe/H].

The Li abundance was derived from the resonance line at 6708 Å, while the subordinated Li line at 6103 Å is not detected. The 3D-NLTE correction by Wang et al. (2021) was applied to the Li abundance, leading to a final abundance of A(Li)$_{\rm NLTE}$=+2.09±0.07, which is consistent with the value quoted by Jacobson et al. (2015): A(Li)$_{\rm NLTE}$=+1.97 dex. The NLTE correction for this star is of +0.04 dex.

The sodium abundance was derived from the Na D lines at 5890 and 5896 Å, which are the only Na transitions visible in the spectrum because of the very low metallicity of the star (Yong et al. 2013 and Jacobson et al. 2015 also derived the Na abundance of HE 0057-5959 measuring these two lines only). We checked that the Na D lines are not contaminated by Na interstellar lines because of the high RV of the star (see Fig. D.1). The NLTE corrections for Na abundance by Lind et al. (2011) were applied, leading to [Na/Fe]=+1.92±0.08 dex, in agreement with the values listed by Yong et al. (2013) and Jacobson et al. (2015). The Na doublet at 5682-88 Å is too weak to be observed, and we can only derive an upper limit of [Na/Fe]<2.1 dex. Figure 1 shows the best-fit synthetic spectra obtained for Li and Na lines as examples.

3. The evolutionary stage of HE0057-5959

Jacobson et al. (2015) derived A(Li)$_{\rm NLTE}$ for a sample of 24 metal-poor giant stars, including HE 0057-5959. All these stars are fainter than that of the RGBb (with a $T_{\rm eff}$ between ~4700 and ~5400 K), and therefore they are not affected by the extra-mixing episode associated with the RGBb. The sample stars have a very similar A(Li)$_{\rm NLTE}$ of around +1.0 dex, which matches the values observed by Mucciarelli et al. (2022) for stars in the same evolutionary stage well. In the Jacobson et al. (2015) sample, HE 0057-5959 is a clear outlier, with a significantly higher Li abundance (A(Li)$_{\rm NLTE}$=+1.97 dex), despite it having only a slightly higher $T_{\rm eff}$ and lower log($L/L_{\odot}$) than the other sample stars. Jacobson et al. (2015) quoted $T_{\rm eff}$ = 5413 K for this star, while the hottest star in the remaining sample has $T_{\rm eff}$ = 5260 K and A(Li)$_{\rm NLTE}$ = 1.21 dex. They do not recognise HE 0057-5959 as an Li-rich star, claiming that this star has an A(Li) depletion

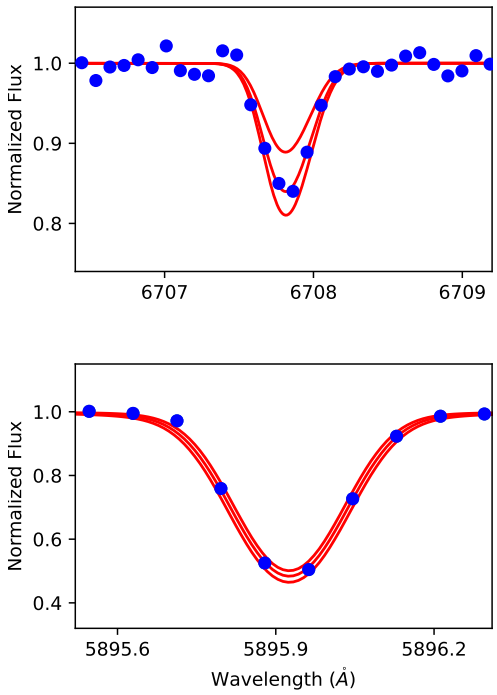

Fig. 1. Spectral regions of MIKE spectrum (blue points) around the Li resonance line and a Na D line (upper and lower panel, respectively), with superimposed synthetic spectra calculated with the best-fit abundance (central red curve) and ±0.1 dex from the best-fit abundance.

level appropriate for its $T_{\rm eff}$. In other words, they interpret this star as an Li-normal star with a high A(Li)$_{\rm NLTE}$ due to an ongoing FDU, the only mechanism able to justify the measured A(Li)$_{\rm NLTE}$ without invoking an anomalous enhancement of Li.

Stellar parameters and A(Li)$_{\rm NLTE}$ from our new analysis agree with those by Norris et al. (2013) and Jacobson et al. (2015), and we confirm that HE 0057-5959 belongs to the first ascent of the RGB (see left panel of Fig. 2). The luminosity of the target is fainter than the RGBb (occurring at $\log(L/L_{\odot})\sim2.35$ for the metallicity of the star; see left panel of Fig. 2.), confirming that HE 0057-5959 is not affected by the extra-mixing episode associated with the RGBb. In order to establish whether its A(Li)$_{\rm NLTE}$ is compatible with an ongoing FDU, we compared the A(Li)$_{\rm NLTE}$ of HE 0057-5959 with that predicted by a theoretical model (calculated with the same code and input physics as in Pietrinferni et al. 2021) of a star with 0.76 $M_{\odot}$ and Z=3.3×10^{-6} (corresponding to [Fe/H]=–4.0 dex and [α/Fe]=+0.4 dex) and without atomic diffusion.

As is clearly visible in the left panel of Fig. 2, at this metallicity the drop of A(Li) due to the FDU occurs at the end of the sub-giant branch. It is confined to a narrow region in $T_{\rm eff}$ of 5500–5800 K and $\log(L/L_{\odot})$, 0.8–1.0. The stellar parameters of HE 0057-5959, within their uncertainties, are not compatible with the position of the FDU, and they indicate that the star has already finished the FDU. The same conclusion is reached whether or not the stellar parameters derived by Norris et al. (2013) and Jacobson et al. (2015) are adopted (see Sect. 2.2). If we assume that this star before the FDU had an A(Li)$_{\rm NLTE}$ similar to that of the Spite Plateau stars (~2.2–2.3 dex), the measured abundance (A(Li)$_{\rm NLTE}$ =+2.09 dex) should be observed when the star starts its FDU, at a $T_{\rm eff}$ hotter by ~300–400 K and a $\log(L/L_{\odot})$ fainter by 0.4 dex with respect to those of HE 0057-5959. Therefore, the measured A(Li)$_{\rm NLTE}$ of HE 0057-5959 is not compatible with what we expect for a star in that evolutionary stage starting from the Spite Plateau. Also, A(Li)$_{\rm NLTE}$ of HE 0057-5959 is clearly incompatible with the abundances of lower RGB stars that share a very similar A(Li) close to +1.0 dex (see right panel of Fig. 2). Hence, we revise our conclusion on the nature of HE 0057-5959 and claim that it is a genuine Li-rich star with a Li abundance significantly higher than those measured in stars at the same evolutionary stage and not compatible with an ongoing FDU. This is the most metal-poor, Li-rich star discovered to date, followed by the giant star LAMOST J070542.30+255226.6, which has [Fe/H]=–3.12 dex (Li et al. 2018).

4. Metal-poor, Li-rich stars in the literature

In order to properly compare the properties of HE 0057-5959 with those of other Li-rich stars, we collected a database of all the metal-poor ([Fe/H]<–1.0 dex) Li-rich stars discovered in our Galaxy to date, making an effort to homogenise their stellar parameters and A(Li)$_{\rm NLTE}$. Adopting for each star the literature stellar parameters and LTE A(Li) derived from the 6708 Å line, we calculated the corresponding synthetic profile and its equivalent width by integration. After that, we calculated the curve of growth for the Li line assuming the new stellar parameters, and we derived the new A(Li) based on the previous equivalent width. The average difference between the LTE A(Li) values obtained with the new and literature parameters are +0.01±0.03 dex (σ=0.18 dex), with only three stars having an absolute discrepancy larger than 0.3 dex. Excluding these three stars, the average difference is +0.04±0.02 dex (σ=0.12 dex). For all the stars, we applied the 3D-NLTE corrections of Wang et al. (2021). Tables E.1 and E.2 list the new $T_{\rm eff}$, $\log -g$, $\log(L/L_{\odot})$, A(Li)$_{\rm NLTE}$, and the literature values of [Fe/H] and [Na/Fe] for all the targets. The positions of all the metal-poor, Li-rich stars in the Hertzsprung-Russell diagram are shown in Fig. 3, where we highlight the mean loci of the FDU and RGBb. We also show two theoretical isochrones with ages of 13 Gyr and [Fe/H]=–3.2 and –1.2 dex (Pietrinferni et al. 2021) as a reference to identify the evolutionary stage of the Li-rich stars.

4.1. Galactic-field Li-rich stars

Aside from HE 0057-5959, 34 metal-poor, Li-rich stars (all of them with A(Li)$_{\rm NLTE}$ higher than the average A(Li) measured in stars at the same evolutionary stage) have been discovered in the Milky Way field, which covers a metallicity range between [Fe/H]~–3.1 and ~–1.4 dex. All these stars were recovered in the *Gaia* eDR3 catalogue, and their parameters ($T_{\rm eff}$, $\log -g$ and $\log(L/L_{\odot})$) were derived using the approach described in Sect. 2. We adopted the colour excess from the latest 3D dust extinction maps by Lallement et al. (2022) for the closest targets, and values from Schlafly & Finkbeiner (2011) for targets whose distance is outside the maps of Lallement et al. (2022). The uncertainties in $T_{\rm eff}$ are dominated by the precision of the adopted colour-$T_{\rm eff}$ transformation (~80 K; see Mucciarelli et al. 2021a), with a negligible contribution arising from photometric error and reddening. The uncertainties in $\log(L/L_{\odot})$ are under 0.1 dex and dominated by the distance error. Only for four stars (namely SDSS J093627.44+293535.7, 2MASS J10122548-2030068, 2MASS J16070923+0447126, and SDSS J143207.14+081406.1) errors in $\log(L/L_{\odot})$ are higher than 0.2 dex, reflecting their large uncertainty in the *Gaia* parallaxes. For seven stars for which $\log -g$ is under 1.3 (the boundary of the grid by Wang et al. 2021), we adopted $\log -g$=1.3 to calculate the 3D-NLTE correction.

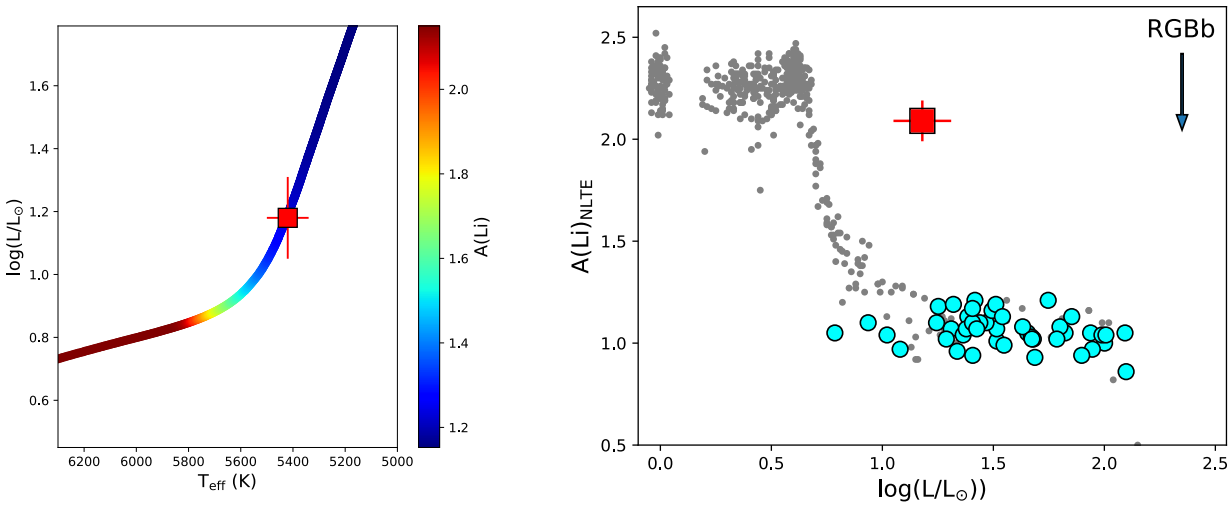

Fig. 2. The evolutionary stage and the surface A(Li) of HE 0057-5959 . Left panel: position of target star HE 0057-5959 in the Hertzsprung-Russell diagram (red square) in comparison with the theoretical track of a star with 0.76 $M_{\odot}$, [Fe/H]=–4.0 dex and [α/Fe]=+0.4 dex, coloured according to the predicted A(Li). The colour-scale is shown on the right side. The model is re-scaled in order to match the average A(Li)$_{\rm NLTE}$ of the RGB stars by Mucciarelli et al. (2022). Right panel: A(Li)$_{\rm NLTE}$ as function of log($L/L_{\odot}$) for HE 0057-5959 (red square) in comparison with the RGB star sample by Mucciarelli et al. (2022, cyan circles) and the stars of the metal-poor ([Fe/H]~–2.0 dex) globular cluster NGC 6397 (Lind et al. 2009, grey circles). The luminosity level of the RGBb for the metallicity of HE 0057-5959 is marked with an arrow.

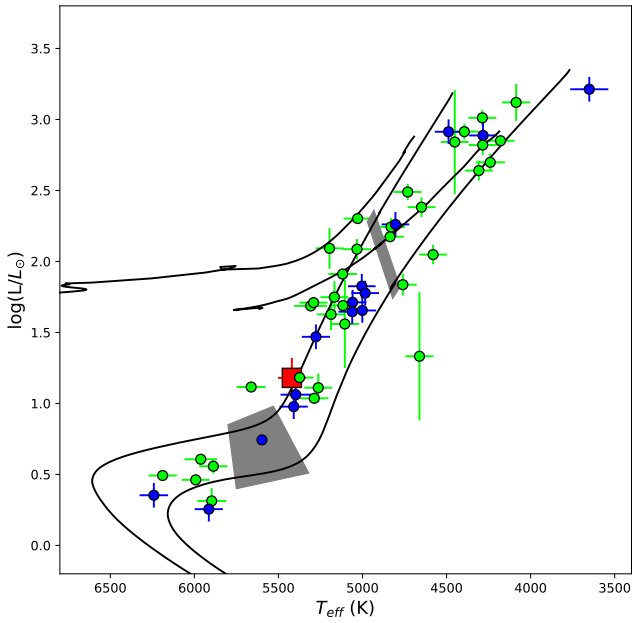

Fig. 3. Position in Hertzsprung-Russell diagram of the target star HE 0057-5959 (red square) and of the other metal-poor ([Fe/H]<–1 dex) Li-rich stars discovered so far (see details in Sect. 4): green circles are Galactic-field stars and blue circles are globular-cluster stars. Two theoretical isochrones with [Fe/H]=–3.2 and –1.2 dex, an α-enhanced chemical mixture, and an age of 13 Gyr (Pietrinferni et al. 2021) are shown for reference (black curves). The two grey shaded areas indicate the loci where the drops of A(Li)$_{\rm NLTE}$ due to the FDU and further extra-mixing episodes, respectively, occur.

The new parameters are in good agreement with the literature ones, with average differences (this study - literature) of +19±23 K (σ=137 K) for $T_{\rm eff}$ and +0.02±0.03 (σ=0.20) for log $-g$. The largest differences are in $T_{\rm eff}$ for the stars LAMOST J055408.54+523559.0, LAMOST J075816.39+470343.3 (Li et al. 2018), 2MASS J05241392-0336543 (Kowkabany et al. 2022), and UCAC4 212-183136 (Susmitha et al. 2024), with differences of –330, –254, –300 K, and +228 K, respectively.

4.2. Galactic globular clusters' Li-rich stars

Sixteen Li-rich stars have been discovered so far in Galactic GCs. We recovered 15 of them in the *Gaia* catalogue, excluding the cepheid star V42 in M5 (Carney et al. 1998) because its variability leads to large uncertainties in the stellar parameters. Three Li-rich stars have a double identification: Stet-M68-S232 in M68 (Ruchti et al. 2011; Kirby et al. 2016), M3-IV 101 in M3 (Kraft et al. 1999; Ruchti et al. 2011), and 132 in M30 (Kirby et al. 2016; Gruyters et al. 2016). Their stellar parameters were derived adopting [Fe/H], and the distance and E(B-V) of Harris (1996, 2010 edition), except for the two Li-rich stars in ω Centauri (Mucciarelli et al. 2019) for which we adopted their proper [Fe/H] values. For the Li-rich stars in NGC 1261 and NGC 6397, we assumed A(Li)=4.0 dex to avoid extrapolation in the 3D-NLTE grids. For the other three stars (namely M3-IV in M3, Stet-M68-S232 in M68, and V2 in NGC 362) we assumed log $-g$= 1.3 as explained above for the field Li-rich stars.

The *Gaia* $T_{\rm eff}$ are in good agreement with the values quoted in the literature, with an average difference of +11±30 K (σ=116 K) and no relevant outliers aside from the cold star V2 in NGC 362 (Smith et al. 1999), which we found to be 250 K cooler. Concerning log $-g$, the average difference is +0.06±0.04 (σ=0.17); most of the targets have differences in log $-g$ within ±0.1, with three main exceptions. These are V2 in NGC 362, which has a log $-g$ that is lower than the Smith et al. (1999) value by 0.4 dex; and 97 812 in NGC 3201 (Aguilera-Gómez et al. 2022) and M3-IV in M3 (Ruchti et al. 2011), which have log $-g$ values that are higher than those in the literature by 0.4 dex.

5. Discussion

5.1. The Li-rich star HE 0057-5959

The star HE 0057-5959 discussed in this work is the most metal-poor, Li-rich star identified to date. We investigated the origin

of its Li enhancement. We considered the main mechanisms previously proposed to explain Li-rich stars.

Concerning the scenario of internal Li production, the main issue for this star is the lack of an internal mixing process able to activate the Cameron-Fowler mechanism. Due to the low metallicity of the star, its shallow convective envelope cannot reach the layers where ^{7}Be is produced through α captures on ^{3}He, and this region is not in contact with the surface, preventing any internal mixing. Possible extra mixing mechanisms can occur in low-mass stars, but this is at the RGBb (Charbonnel & Balachandran 2000; Palacios et al. 2001) or close to the He flash (Silva Aguirre et al. 2014), while this star is located at the base of the RGB.

Mass-transfer processes from a more massive, now evolved, companion star able to produce fresh Li via the Cameron-Fowler mechanism is a valuable and simple route to explain Li-rich stars. The measured RV from our MIKE spectrum nicely matches the previous estimates indicating no large RV variations. The RUWE value of the star is 0.98, indicating a well-behaved single-star astrometric solution. However, wide binary systems may have periods that are too long to be identified with the *Gaia* observations. We cannot totally rule out the star belonging to a long-period or highly inclined binary. In this case, the enhancement of Li could be explained as the result of a mass-transfer process from a more massive companion star during its AGB stage. We note that none of the Li-rich stars for which multiple epochs are available has shown evidence of variability, with the only exception being 25 664 in ω Centauri (Mucciarelli et al. 2021b).

The Li overabundance in a giant star can be the result of engulfment of a planet as the star evolves on the RGB, thus increasing its radius. This seems to be the most likely explanation for the solar metallicity of the Li-rich giant BD+48 740 (Adamów et al. 2012). However, the extremely low metallicity of HE 0057-5959 makes it unlikely for it to host, or have hosted, planets. In spite of early claims that the frequency of planets around giant stars is not correlated with metallicity (Pasquini et al. 2007), subsequent investigations found that the higher the metallicity, the higher the probability of hosting a planet (Wolthoff et al. 2022, and references therein), similar to what was found for dwarf stars, see Adibekyan (2019) and references therein. To our knowledge, the two planet-host stars with the lowest metallicity are BD+20 2457 (Maldonado et al. 2013) and 24 Boo (Takarada et al. 2018), both of which have metallicities around –0.8 dex. Clearly, if we were to extrapolate this metallicity dependence of hosting planets down to –4.0 dex, we would find a very low number (practically zero). One should keep in mind, however, that the stars with metallicities below –3.0 dex are not represented in any of the planet search surveys; thus, such an extrapolation cannot be supported by any data. We nevertheless believe that, based on our current knowledge, the possibility of the high Li abundance in HE 0057-5959 being due to planet engulfment can be discarded.

In conclusion, the mass-transfer scenario remains the most promising one, lacking a well established mechanism capable of inducing a Cameron-Fowler mechanism in a low-mass, very metal-poor stars such as HE 0057-5959. Whatever mechanism is capable of generating an Li-rich star, that mechanism must also occur down to [Fe/H]∼–4 dex.

5.2. An overview of the metal-poor, Li-rich stars

We discuss the properties of HE 0057-5959 in comparison with the other metal-poor ([Fe/H]<–1 dex) Li-rich stars (see Sect. 4). The vast majority of the low-mass dwarf stars in the metallicity range between [Fe/H]∼–3 and ∼–1 dex share a similar abundance: A(Li)$_{\rm NLTE}$ ∼2.2–2.3 dex. At higher metallicities, two effects occur: destruction of the plateau and the significant increase of the star-to-star scatter. The first one is the presence of more massive convective envelopes in these stars, which leads to more efficient surface A(Li) depletion (Meléndez et al. 2014). The second effect is the occurrence of novae that produce fresh Li and contribute to the chemical enrichment of the Galaxy for [Fe/H]>–1 dex (see e.g. Izzo et al. 2015; Romano et al. 2021; Izzo et al. 2023). In fact, following the detection in RS Oph (Molaro et al. 2023), we know that recurrent novae also contribute to the Li production. In this way, the interpretation of metal-poor, Li-rich stars has the advantage of removing the effects of the extra dilution due to the massive convective envelope and the effect of novae producing additional Li from the discussion.

In principle, the A(Li) of an Li-rich star (regardless of its origin) should follow the same evolutionary path of an Li-normal star, with a significant reduction at the FDU and the RGBb. For this reason, Li-rich stars should be discussed considering their evolutionary stage and the possible occurrence of the mixing episodes.

The upper left panel of Fig. 4 shows the run of A(Li)$_{\rm NLTE}$ as a function of $\log(L/L_\odot)$ for HE 0057-5959 and all the other metal-poor, Li-rich stars discovered to date. Despite a significant star-to-star scatter, it is possible to recognise some sequences where A(Li) decreases with increasing $\log(L/L_\odot)$. Some of the field Li-rich stars draw a clear sequence starting from A(Li)∼3.2 dex at $\log(L/L_\odot)$ ∼+0.5 down to A(Li)∼2.2 dex at $\log(L/L_\odot)$ ∼+2. The GC Li-rich stars in the same luminosity range seem to draw a parallel sequence, but it is shifted by 0.4 dex towards lower A(Li). Finally, some field and GC stars define a super Li-rich sequence, with values higher than the other Li-rich stars of similar $\log(L/L_\odot)$ by 1 dex. Two sequences of A(Li) as a function of $\log(L/L_\odot)$ for the GC Li-rich stars have already been proposed by Sanna et al. (2020). We note that the Li-rich stars show a decrease of A(Li) that is less steep than that expected by the FDU.

The other panels of Fig. 4 show the behaviour of A(Li)$_{\rm NLTE}$ as a function of [Fe/H] for the stars grouped according to their evolutionary stages. In particular, we consider stars located before the FDU (corresponding to the Spite Plateau for Li-normal stars), after the FDU and before the RGBb (corresponding to the lower RGB plateau for Li-normal stars), and after the RGBb (stars experienced the extra mixing episode at the luminosity level of the RGBb). Only one Li-rich star, namely 132 in the GC M30, is clearly located during the FDU (see Fig. 2 and Table E.2) and excluded from this discussion. Also, two field stars (namely GSC 03797-00204 and 2MASS J19524490-6008132) are close the RGBb, and we propose an attempt at classification (they are marked as empty symbols in Fig. 4; see Table E.1). Finally, for two stars (namely SDSS J143207.14+081406.1 and 2MASS J04315411-0632100) the attribution is too uncertain due to their anomalous position in the Hertzsprung-Russell diagram (see Fig. 3).

Seven Li-rich stars (two of them members of GCs) are located before the occurrence of the FDU. Six of them have A(Li)$_{\rm NLTE}$ exceeding the primordial value obtained from the standard Big Bang nucleosynthesis model and the Planck/WMAP measurements of the baryon density. Among them, four stars have A(Li)$_{\rm NLTE}$∼3–3.2 dex (about 1 dex higher than the Spite Plateau), and the other two stars have A(Li)$_{\rm NLTE}$∼4 dex (about 2 dex higher than the Spite Plateau).

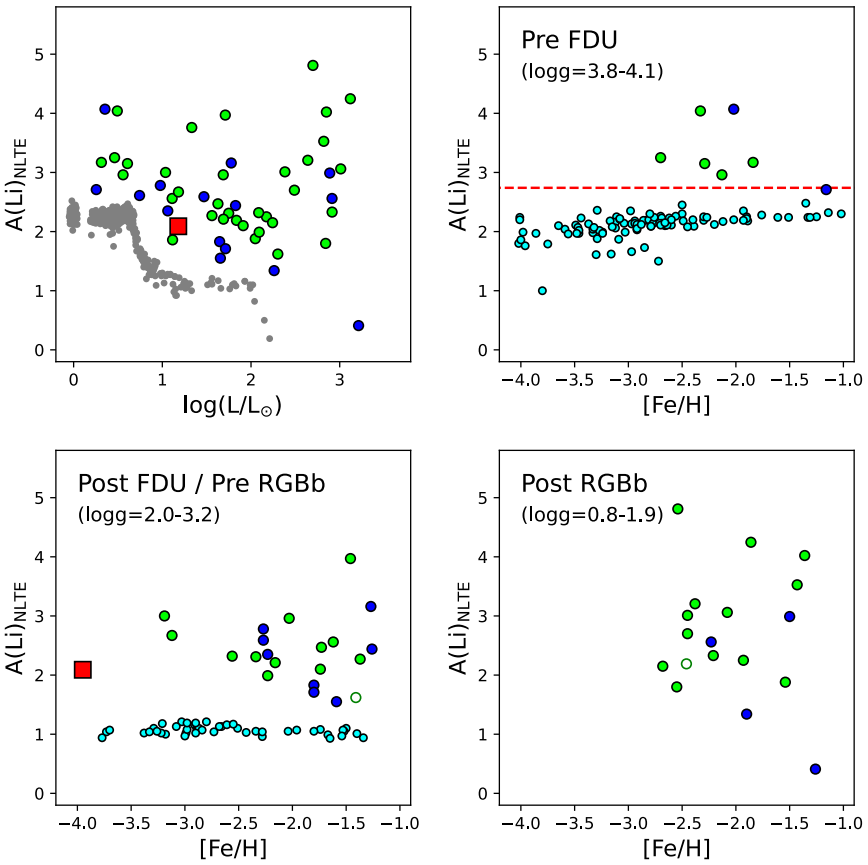

Fig. 4. Surface A(Li) of the Li-rich stars discovered so far. Upper left panel: behaviour of $A(Li)_{NLTE}$ as function of $\log(L/L_{\odot})$ for all the metal-poor ([Fe/H]<–1 dex) Li-rich stars discovered so far. Green circles are Milky Way field stars, blue circles are globular-cluster stars, and the red squares mark HE 0057-5959. The stars of the metal-poor ([Fe/H]~–2.0 dex) globular cluster NGC 6397 (grey circles, Lind et al. 2009) are shown as a reference (and to identify the luminosity of the FDU and RGBb). Upper right panel: run of $A(Li)_{NLTE}$ as function of [Fe/H] for the Li-rich stars located before the FDU. Red dashed line indicates the WMAP/SBNN A(Li) (Coc & Vangioni 2017). The cyan circles are Li-normal Milky Way field stars (Ryan et al. 1999; Lucatello et al. 2003; Ivans et al. 2005; Asplund et al. 2006; Sivarani et al. 2006; Thompson et al. 2008; Sbordone et al. 2010; Masseron et al. 2012; Ito et al. 2013; Hansen et al. 2014; Bonifacio et al. 2015; Li et al. 2015; Placco et al. 2016; Matsuno et al. 2017; Aguado et al. 2018; Bonifacio et al. 2018). Lower-left panel: run of $A(Li)_{NLTE}$ as function of [Fe/H] for the Li-rich stars located after the completion of FDU and before the RGBb. The open circle indicates the star 2MASS J19524490-6008132 with an uncertain attribution to this group. The cyan circles are Li-normal Milky Way field stars (Mucciarelli et al. 2022). Lower right panel: run of $A(Li)_{NLTE}$ as function of [Fe/H] for the Li-rich stars located after the RGBb. Open circle indicates the star GSC 03797-00204 with an uncertain attribution to this group.

Only the Li-rich star in M 4 (Monaco et al. 2012) has a value compatible with the primordial value.

Twenty-one stars are located between the completion of the FDU and before the RGBb. They show a large A(Li) scatter and a typical value around +2.4 dex, which is 1.4 dex higher than the abundances measured along the lower RGB plateau. However, their average value is lower than that measured in the previous group, suggesting that a dilution due to the FDU occurred.

Eighteen stars (4 of them members of GCs) are located after the RGBb. In this group, we found the Li-rich stars with the lowest (Smith et al. 1999) and the highest (Kowkabany et al. 2022) $A(Li)_{NLTE}$ of the entire sample. The average value of these stars matches that of the stars between the FDU and the RGBb well.

For the stars between FDU and the RGBb, we corrected the measured $A(Li)_{NLTE}$ to take into account the effect of the Li dilution due to the FDU, following the method described in Mucciarelli et al. (2012). In particular, for each star in this evolutionary stage, we consider the stellar model with the appropriate metallicity that provides the amount of A(Li) dilution as a function of the stellar luminosity. The A(Li) dilution to be added to the measured $A(Li)_{NLTE}$ value is computed according to the $\log(L/L_{\odot})$ value of each star. This approach is restricted to stars experiencing the FDU, but fainter than the RGBb, because the standard stellar-evolution models that we adopted do not account for non-canonical mixing processes.

Figure 5 shows the run of the corrected A(Li) with [Fe/H] for these stars, together with the (uncorrected) abundances for stars before the FDU. No evident trend between the initial A(Li) and [Fe/H] is found. The derived distribution exhibits a large star-to-star scatter, and almost all the stars (assuming that they formed with a high A(Li)) have abundances higher than the cosmological value. For the target star, HE 0057-5959, the predicted initial A(Li) should be +3.05 dex, which is ~0.3 dex higher

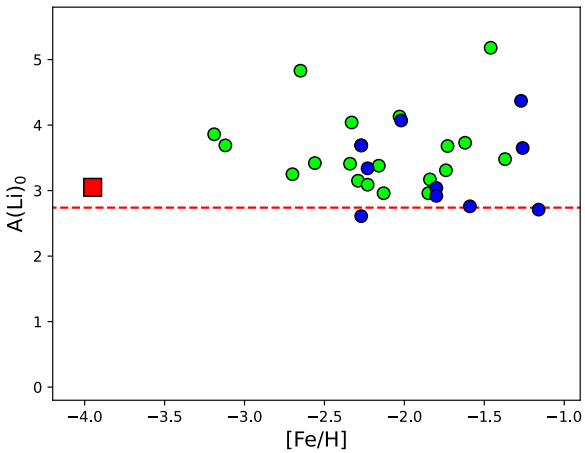

Fig. 5. Behaviour of initial A(Li), accounting for the dilution effect due to the FDU, for HE 0057-5959 and other metal-poor, Li-rich stars fainter than the RGBb (same symbols as Fig. 3).

than the cosmological value. Only a few stars could have an initial A(Li) compatible with the cosmological value (which could be explained by invoking some preservation of the pristine Li), while for most of the Li-rich stars, processes able to produce or enhance the surface A(Li) should occur.

5.3. HE 0057-5959: An Na-rich Li-rich metal-poor star

Previous works on metal-poor, Li-rich stars highlighted significant over-abundances of [Na/Fe] in some of them (see e.g. Kowkabany et al. 2022; Sitnova et al. 2023) but this chemical signature has not been properly discussed. Na abundances are

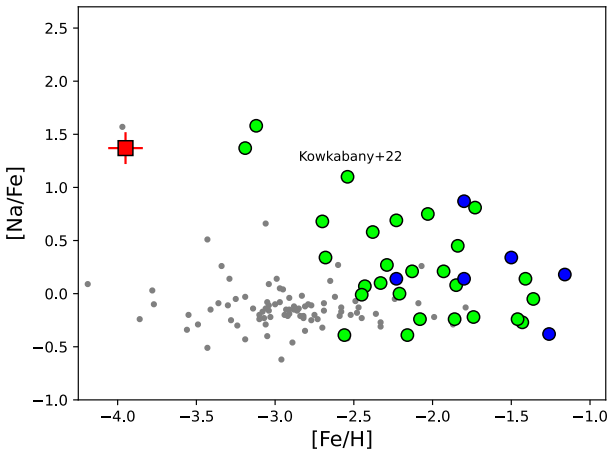

Fig. 6. Behaviour of [Na/Fe] as function of [Fe/H] of the metal-poor, Li-rich stars (same symbols of Fig. 3) in comparison with the NLTE abundances for metal-poor Milky Way stars (grey circles) from Andrievsky et al. (2007) and Lombardo et al. (2022). The [Na/Fe] abundance ratio of HE 0057-5959 plotted here accounts for NLTE effects for Na abundance only. The position of the Li-rich star by Kowkabany et al. (2022), the most Li-rich discovered so far, is marked.

available for 23 field stars, as shown in Fig. 6 in comparison with the metal-poor Milky Way field stars (Andrievsky et al. 2007; Lombardo et al. 2022). We also show the six GC Li-rich stars with [Na/Fe] abundances even if the discussion of these stars is complicated by the self-enrichment processes occurring in the early epochs of the GC life, and these stars are likely able to form new stars with excesses of [Na/Fe] (see e.g. Bastian & Lardo 2018). In the following, we only refer to the field Li-rich stars.

The [Na/Fe] distribution of the metal-poor, Li-rich stars does not match that of the Milky Way field stars. For [Fe/H]<–2.0 dex, the field stars have a constant value of [Na/Fe]~–0.2 dex, while the Li-rich stars exhibit a significant star-to-star scatter in [Na/Fe], reaching very high values up to [Na/Fe]~+1.6 dex. In particular, the three Li-rich stars with [Fe/H]<–3.0 dex have [Na/Fe]>+1.3 dex and are the most Na-rich Li-rich stars: HE 0057-5959, with [Na/Fe]=+1.37 dex; *Gaia* EDR3 883042050539140992, with [Na/Fe]=+1.37 dex (Li et al. 2018); and *Gaia* EDR3 2604066644687553792, with [Na/Fe]=+1.58 dex (Roederer et al. 2014). In this comparison and in Fig. 6 we used [Na/Fe]=+1.37 for HE 0057-5959, which was obtained by adopting NLTE Na abundance and LTE Fe abundance, similarly to the analyses of other Li-rich stars, where only the Na abundances are corrected for NLTE effects.

Even though only three Li-rich stars with [Fe/H]<–3 dex have been discovered to date, their extremely high [Na/Fe] abundance ratios could be a new characteristic feature of this class of rare objects thus far unexplored. Sodium is produced in both massive stars during the hydrostatic C and Ne burning and in AGB stars during the hot bottom-burning phase. In particular, super-AGB stars with initial masses larger than ~6–7 $M_{\odot}$ should be able to produce large amounts of both Li and Na (at least for [Fe/H]>–2.5 dex; e.g. Ventura & D'Antona 2011; D'Antona et al. 2012; Doherty et al. 2014). In these stars, Li is produced through the Cameron-Fowler mechanism, and Na is produced through the Ne-Na cycle. The evidence that all three Li-rich stars with [Fe/H]<–3 dex have an excess of [Na/Fe] could be an important hint supporting the scenario of a mass-transfer process occurring in binary systems where the companion was a massive star able to produce Li and Na simultaneously. Unfortunately, theoretical models for AGB stars at [Fe/H]=–4 dex are not yet available.

6. Conclusions

We revised the nature of the metal-poor star HE 0057-5959, demonstrating that it is a genuine Li-rich star and that it belongs to the limited class of the metal-poor, Li-rich stars. Its very low metallicity demonstrates that at least one of the proposed mechanisms able to produce Li-rich stars should work down to [Fe/H]~–4 dex. However, we are not yet able to identify the process capable of producing the excess Li observed in this star and generally in other metal-poor stars with absolute certainty. This is due to our still only partial understanding of the properties of these stars and to the lack of a sound mechanism capable of triggering the Cameron-Fowler mechanism in many of these stars (especially those fainter than the RGBb). For the star HE 0057-5959, we can only speculate that the excess of Li may be attributable to a mass-transfer process in a binary system, despite not having strong evidence of this, except perhaps for the very high [Na/Fe] supporting this hypothesis. The extremely high Li and Na abundances could be compatible with a mass transfer from a companion in the stellar range of 6–8 $M_{\odot}$, while the lack of RV variations from the three available epochs and the RUWE *Gaia* parameter close to the unity do not support the binary nature of the star (but neither do they rule out a long-period binary system). On the other hand, HE 0057-5959 does not exhibit any enhancement of neutron-capture elements (Sr and Ba) usually associated with the mass-transfer process from AGB stars. However, it is important to bear in mind that AGB stars of 2–4 $M_{\odot}$ produce a large amount of neutron-capture elements, while stars with 6–8 $M_{\odot}$ are much less efficient in producing these elements (see e.g. Fishlock et al. 2014; Shingles et al. 2015). Therefore, all the chemical evidence collected so far for HE 0057-5959 is in agreement with this scenario.

Detailed chemical abundances of the main groups of elements are limited to a few stars; in particular, elements that are tracers of mass transfer from AGB stars (i.e. CNO, $^{12}C/^{13}C$, and neutron-capture processes) are simultaneously available for only nine Li-rich stars. Another missing piece of evidence includes dedicated surveys of RV in order to monitor possible variability and establish the binary nature of some of these stars. In the same way, systematic studies of other diagnostics of interactions (chromospheric activity, stellar rotation...) are still lacking. Metal-poor, Li-rich stars therefore belong to an unexplored field of research that deserves deeper investigation.

Acknowledgements. We thanks the anonymous referee for the useful and constructive suggestions. A.M. acknowledges support from the project "LEGO – Reconstructing the building blocks of the Galaxy by chemical tagging" (PI: A. Mucciarelli). granted by the Italian MUR through contract PRIN 2022LLP8TK_001. M.M. acknowledges support from the ERC Consolidator Grant funding scheme (project ASTEROCHRONOMETRY, https://www.asterochronometry.eu, G.A. n. 772293). This work has made use of data from the European Space Agency (ESA) mission *Gaia* (https://www.cosmos.esa.int/gaia), processed by the *Gaia* Data Processing and Analysis Consortium (DPAC, https://www.cosmos.esa.int/web/gaia/dpac/consortium). Funding for the DPAC has been provided by national institutions, in particular the institutions participating in the *Gaia* Multilateral Agreement. This research has made use of the SIMBAD database, operated at CDS, Strasbourg, France.

References

Adamów, M., Niedzielski, A., Villaver, E., et al. 2012, ApJ, 754, L15
Adibekyan, V. 2019, Geosciences, 9, 105

Aguado, D. S., Allende Prieto, C., González Hernández, J. I., et al. 2018, ApJ, 854, L34
Aguilera-Gómez, C., Monaco, L., Mucciarelli, A., et al. 2022, A&A, 657, A33
Andrievsky, S. M., Spite, M., Korotin, S. A., et al. 2007, A&A, 464, 1081
Arentsen, A., Starkenburg, E., Shetrone, M. D., et al. 2019, A&A, 621, A108
Asplund, M., Lambert, D. L., Nissen, P. E., et al. 2006, ApJ, 644, 229
Asplund, M., Grevesse, N., Sauval, A. J., et al. 2009, ARA&A, 47, 481
Aoki, W., Beers, T. C., Sivarani, T., et al. 2008, ApJ, 678, 1351
Aoki, W., Barklem, P. S., Beers, T. C., et al. 2009, ApJ, 698, 1803
Bailer-Jones, C. A. L., Rybizki, J., Fouesneau, M., et al. 2021, AJ, 161, 147
Bastian, N., & Lardo, C. 2018, ARA&A, 56, 83
Bergemann, M., Kudritzki, R.-P., Würl, M., et al. 2013, ApJ, 764, 115
Bernstein, R., Shectman, S. A., Gunnels, S. M., et al. 2003, Proc. SPIE, 4841, 1694
Bonifacio, P., & Molaro, P. 1997, MNRAS, 285, 847
Bonifacio, P., Caffau, E., Spite, M., et al. 2015, A&A, 579, A28
Bonifacio, P., Caffau, E., Spite, M., et al. 2018, A&A, 612, A65
Caffau, E., Ludwig, H.-G., Steffen, M., et al. 2011, Sol. Phys., 268, 255
Cameron, A. G. W. 1955, ApJ, 121, 144
Cameron, A. G. W., & Fowler, W. A. 1971, ApJ, 164, 111
Carney, B. W., Fry, A. M., & Gonzalez, G. 1998, AJ, 116, 2984
Casey, A. R., Ruchti, G., Masseron, T., et al. 2016, MNRAS, 461, 3336
Charbonnel, C., & Balachandran, S. C. 2000, A&A, 359, 563
Charbonnel, C., & Primas, F. 2005, A&A, 442, 961
Charbonnel, C., Lagarde, N., Jasniewicz, G., et al. 2020, A&A, 633, A34
Coc, A., & Vangioni, E. 2017, Int. J. Mod. Phys. E, 26, 1741002
D'Antona, F., D'Ercole, A., Carini, R., et al. 2012, MNRAS, 426, 1710
Deepak, Lambert, D. L., & Reddy, B. E. 2020, MNRAS, 494, 1348
de La Reza, R., Drake, N. A., & da Silva, L. 1996, ApJ, 456, L115
Denissenkov, P. A., & Herwig, F. 2004, ApJ, 612, 1081
Denissenkov, P. A., Pinsonneault, M., & MacGregor, K. B. 2009, ApJ, 696, 1823
Doherty, C. L., Gil-Pons, P., Lau, H. H. B., et al. 2014, MNRAS, 441, 582
Domínguez, I., Abia, C., Straniero, O., et al. 2004, A&A, 422, 1045
D'Orazi, V., Gratton, R. G., Angelou, G. C., et al. 2015, ApJ, 801, L32
Fischer, D. A., & Valenti, J. 2005, ApJ, 622, 1102
Fishlock, C. K., Karakas, A. I., Lugaro, M., et al. 2014, ApJ, 797, 44
Gaia Collaboration (Prusti, T., et al.) 2016, A&A, 595, A1
Gaia Collaboration (Brown, A. G. A., et al.) 2021, A&A, 649, A1
Gao, Q., Shi, J.-R., Yan, H.-L., et al. 2019, ApJS, 245, 33
Gonzalez, O. A., Zoccali, M., Monaco, L., et al. 2009, A&A, 508, 289
Gruyters, P., Lind, K., Richard, O., et al. 2016, A&A, 589, A61
Handberg, R., Lund, M. N., White, T. R., et al. 2021, AJ, 162, 170
Hansen, T., Hansen, C. J., Christlieb, N., et al. 2014, ApJ, 787, 162
Harris, W. E. 1996, AJ, 112, 1487
Hatt, E., Nielsen, M. B., Chaplin, W. J., et al. 2023, A&A, 669, A67
Hon, M., Huber, D., Kuszlewicz, J. S., et al. 2021, ApJ, 919, 131
Huang, C. X., Vanderburg, A., Pál, A., et al. 2020, Res. Notes Am. Astron. Soc., 4, 204
Iben, I. 1967, ApJ, 147, 624
Ito, H., Aoki, W., Beers, T. C., et al. 2013, ApJ, 773, 33
Ivans, I. I., Sneden, C., Gallino, R., et al. 2005, ApJ, 627, L145
Izzo, L., Della Valle, M., Mason, E., et al. 2015, ApJ, 808, L14
Izzo, L., Molaro, P., Bonifacio, P., et al. 2023, Exp. Astron., 55, 191
Jacobson, H. R., Keller, S., Frebel, A., et al. 2015, ApJ, 807, 171
Johnson, J. A., Aller, K. M., Howard, A. W., et al. 2010, PASP, 122, 905
Kelson, D. D. 2003, PASP, 115, 688
Kirby, E. N., Fu, X., Guhathakurta, P., et al. 2012, ApJ, 752, L16
Kirby, E. N., Guhathakurta, P., Zhang, A. J., et al. 2016, ApJ, 819, 135
Koch, A., Lind, K., & Rich, R. M. 2011, ApJ, 738, L29
Kowkabany, J., Ezzeddine, R., Charbonnel, C., et al. 2022, arXiv e-prints [arXiv:2209.02184]
Kraft, R. P., Peterson, R. C., Guhathakurta, P., et al. 1999, ApJ, 518, L53
Kurucz, R. L. 1993, VizieR Online Data Catalog: VI/39
Kurucz, R. L. 2005, Mem. Soc. Astron. It. Suppl., 8, 14
Lallement, R., Vergely, J. L., Babusiaux, C., et al. 2022, A&A, 661, A147
Li, H., Aoki, W., Zhao, G., et al. 2015, PASJ, 67, 84
Li, H., Aoki, W., Matsuno, T., et al. 2018, ApJ, 852, L31
Lightkurve Collaboration (Cardoso, J. V. de M., et al.) 2018, Astrophysics Source Code Library [record ascl:1812.013]
Lind, K., Primas, F., Charbonnel, C., et al. 2009, A&A, 503, 545
Lind, K., Asplund, M., Barklem, P. S., et al. 2011, A&A, 528, A103
Lodders, K. 2010, Astrophys. Space Sci. Proc., 16, 379
Lomb, N. R. 1976, Ap&SS, 39, 447
Lombardo, L., François, P., Bonifacio, P., et al. 2021, A&A, 656, A155
Lombardo, L., Bonifacio, P., François, P., et al. 2022, A&A, 665, A10
Lucatello, S., Gratton, R., Cohen, J. G., et al. 2003, AJ, 125, 875
Lund, M. N., Handberg, R., Buzasi, D. L., et al. 2021, ApJS, 257, 53
Mackereth, J. T., Miglio, A., Elsworth, Y., et al. 2021, MNRAS, 502, 1947
Maldonado, J., Villaver, E., & Eiroa, C. 2013, A&A, 554, A84
Martell, S. L., & Shetrone, M. D. 2013, MNRAS, 430, 611
Mashonkina, L., Pakhomov, Y., Sitnova, T., et al. 2023, MNRAS, 524, 3526
Masseron, T., Johnson, J. A., Lucatello, S., et al. 2012, ApJ, 751, 14
Matsuno, T., Aoki, W., Beers, T. C., et al. 2017, AJ, 154, 52
Meléndez, J., Schirbel, L., Monroe, T. R., et al. 2014, A&A, 567, L3
Molaro, P., Izzo, L., Selvelli, P., et al. 2023, MNRAS, 518, 2614
Monaco, L., Villanova, S., Moni Bidin, C., et al. 2011, A&A, 529, A90
Monaco, L., Villanova, S., Bonifacio, P., et al. 2012, A&A, 539, A157
Monaco, L., Boffin, H. M. J., Bonifacio, P., et al. 2014, A&A, 564, L6
Mucciarelli, A., & Bonifacio, P. 2020, A&A, 640, A87
Mucciarelli, A., Salaris, M., & Bonifacio, P. 2012, MNRAS, 419, 2195
Mucciarelli, A., Pancino, E., Lovisi, L., et al. 2013a, ApJ, 766, 78
Mucciarelli, A., Bellazzini, M., Catelan, M., et al. 2013b, MNRAS, 435, 3667
Mucciarelli, A., Monaco, L., Bonifacio, P., et al. 2019, A&A, 623, A55
Mucciarelli, A., Bellazzini, M., & Massari, D. 2021a, A&A, 653, A90
Mucciarelli, A., Monaco, L., Bonifacio, P., et al. 2021b, A&A, 652, A139
Mucciarelli, A., Monaco, L., Bonifacio, P., et al. 2022, A&A, 661, A153
Nordlander, T., & Lind, K. 2017, A&A, 607, A75
Norris, J. E., Bessell, M. S., Yong, D., et al. 2013, ApJ, 762, 25
Palacios, A., Charbonnel, C., & Forestini, M. 2001, A&A, 375, L9
Pasquini, L., Döllinger, M. P., Weiss, A., et al. 2007, A&A, 473, 979
Pietrinferni, A., Hidalgo, S., Cassisi, S., et al. 2021, ApJ, 908, 102
Placco, V. M., Beers, T. C., Reggiani, H., et al. 2016, ApJ, 829, L24
Ricker, G. R., Winn, J. N., Vanderspek, R., et al. 2015, J. Astron. Telesc. Instrum. Syst., 1, 014003
Roederer, I. U., Frebel, A., Shetrone, M. D., et al. 2008, ApJ, 679, 1549
Roederer, I. U., Preston, G. W., Thompson, I. B., et al. 2014, AJ, 147, 136
Romano, D., Magrini, L., Randich, S., et al. 2021, A&A, 653, A72
Ruchti, G. R., Fulbright, J. P., Wyse, R. F. G., et al. 2011, ApJ, 743, 107
Ryan, S. G., Norris, J. E., & Beers, T. C. 1999, ApJ, 523, 654
Sackmann, I.-J., & Boothroyd, A. I. 1992, ApJ, 392, L71
Sanna, N., Franciosini, E., Pancino, E., et al. 2020, A&A, 639, L2
Sbordone, L., Bonifacio, P., Caffau, E., et al. 2010, A&A, 522, A26
Scargle, J. D. 1982, ApJ, 263, 835
Schlafly, E. F., & Finkbeiner, D. P. 2011, ApJ, 737, 103
Shingles, L. J., Doherty, C. L., Karakas, A. I., et al. 2015, MNRAS, 452, 2804
Siess, L., & Livio, M. 1999, MNRAS, 308, 1133
Silva Aguirre, V., Ruchti, G. R., Hekker, S., et al. 2014, ApJ, 784, L16
Sitnova, T. M., Matsuno, T., Yuan, Z., et al. 2023, MNRAS, 526, 5976
Sivarani, T., Beers, T. C., Bonifacio, P., et al. 2006, A&A, 459, 125
Smith, V. V., Shetrone, M. D., & Keane, M. J. 1999, ApJ, 516, L73
Spite, M., & Spite, F. 1982, Nature, 297, 483
Susmitha, A., Mallick, A., & Reddy, B. E. 2024, ApJ, 966, 109
Takarada, T., Sato, B., Omiya, M., et al. 2018, PASJ, 70, 59
Thompson, I. B., Ivans, I. I., Bisterzo, S., et al. 2008, ApJ, 677, 556
Ventura, P., & D'Antona, F. 2011, MNRAS, 410, 2760
Yong, D., Norris, J. E., Bessell, M. S., et al. 2013, ApJ, 762, 26
Wang, E. X., Nordlander, T., Asplund, M., et al. 2021, MNRAS, 500, 2159
Wolthoff, V., Reffert, S., Quirrenbach, A., et al. 2022, A&A, 661, A63

Appendix A: Asteroseismic data

Here we discuss asteroseismic observations of metal-poor Li-rich stars (Table E.1). Our sample of stars has been observed by TESS (Transiting Exoplanet Survey Satellite; Ricker et al. 2015), but only 16 stars have available light curves in the Mikulski archive for space telescopes (MAST[1]). We apply a Lomb–Scargle transform (Lomb 1976; Scargle 1982) to these lightcurves by means of the Python package LIGHTKURVE v2.4.1[2]. We do not find evidence of solar-like oscillations in any of these stars even with lightcurves based on the MIT quick-look pipeline (QLP; Huang et al. 2020), or the TESS data for asteroseismology light curves pipeline (TASOC; Handberg et al. 2021; Lund et al. 2021). Fig. A.1 shows as example of the power spectral density for HE 0057-5959 based on TESS observations. Indeed, we could not find any of these stars in catalogues of solar-like oscillators observed with TESS (Hon et al. 2021; Mackereth et al. 2021; Hatt et al. 2023), and a similar result is shown in Kowkabany et al. (2022) for the star *Gaia* DR3 3210839729979320064. Finally, these results suggest that more than 130 days (corresponding to longest observations made in our sample, that is those for *Gaia* DR3 3360259919923274496) are needed to observe solar-like oscillations in such stars.

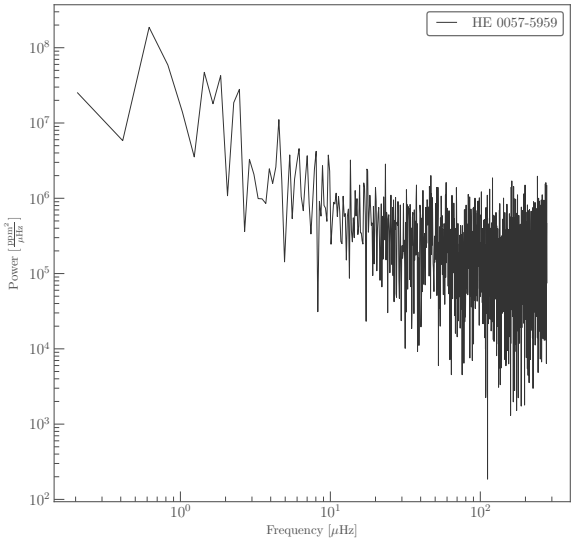

Fig. A.1. Power spectral density for HE 0057-5959 based on TESS observations during Sector 1 and 2. The light curve from which we obtain the power spectral density is provided by the TESS Asteroseismic Science Operations Center (TASOC; Handberg et al. 2021; Lund et al. 2021). We find no evidence of solar-like oscillations.

Appendix B: Information about the measured atomic lines

Table B.1 lists the main atomic data (wavelength, oscillator strength, excitation potential and ion) for all the measured transitions used in the analysis.

[1] https://archive.stsci.edu
[2] Lightkurve Collaboration et al. (2018); https://github.com/lightkurve/lightkurve

Table B.1. Main atomic data for the measured transitions used in the analysis.

Wavelength (Å)	log gf (dex)	χ (eV)	Ion
6707.***	–0.002	0.00	Li I
5889.9**	0.108	0.00	Na I
5895.9**	–0.194	0.00	Na I
3838.292	0.397	2.72	Mg I
5167.321	–0.870	2.71	Mg I
5172.684	–0.393	2.71	Mg I
5183.604	–0.167	2.72	Mg I
3944.***	–0.635	0.00	Al I
3961.5**	–0.333	0.01	Al I
3905.523	–1.041	1.91	Si I
4226.728	0.244	0.00	Ca I
4300.043	–0.460	1.18	Ti II
4563.758	–0.795	1.22	Ti II
4571.971	–0.310	1.57	Ti II
3820.425	0.119	0.86	Fe I
3840.437	–0.506	0.99	Fe I
3841.048	–0.045	1.61	Fe I
3849.966	–0.871	1.01	Fe I
3878.018	–0.914	0.96	Fe I
3878.573	–1.379	0.09	Fe I
3886.282	–1.076	0.05	Fe I
3895.656	–1.670	0.11	Fe I
3902.945	–0.466	1.56	Fe I
3906.479	–2.243	0.11	Fe I
4005.241	–0.610	1.56	Fe I
4202.029	–0.708	1.48	Fe I
4250.786	–0.714	1.56	Fe I
4260.474	0.077	2.40	Fe I
4271.760	–0.164	1.48	Fe I
4325.762	0.006	1.61	Fe I
5227.188	–1.228	1.56	Fe I
5269.537	–1.321	0.86	Fe I
5270.356	–1.339	1.61	Fe I
5371.489	–1.645	0.96	Fe I
5397.127	–1.993	0.91	Fe I
5405.774	–1.844	0.99	Fe I
5446.916	–1.914	0.99	Fe I
4215.519	–0.173	0.00	Sr II
4554.0**	0.140	0.00	Ba II

Appendix C: Comparison with previous chemical analyses

The chemical composition of HE 0057-5959 has been already investigated by Yong et al. (2013) and Jacobson et al. (2015) both analysing MIKE spectra. Fig. C.1 shows the comparison between our analysis and those by Yong et al. (2013) and Jacobson et al. (2015) for the elements in common among the three studies. We consider our LTE abundances but for Li and Na because these two studies provided NLTE abundances only for these two elements. Our analysis well agrees with the previous ones, with differences that do not exceed ±0.2 dex. The largest differences are for the [C/Fe] and [Ca/Fe] by Yong et al. (2013), 0.21 dex lower and higher than our values, respectively. The differences with respect to these two studies can be ascribable to several differences in the chemical analyses, in particular, both the works adopted solar abundances by Asplund et al. (2009), Jacobson et al. (2015) used MARCS model atmospheres, while

Yong et al. (2013) adopted ATLAS9 model atmospheres like our analysis, and Yong et al. (2013) adopted a $T_{\rm eff}$ value ~200 K cooler than our one (see Sect. 2.2).

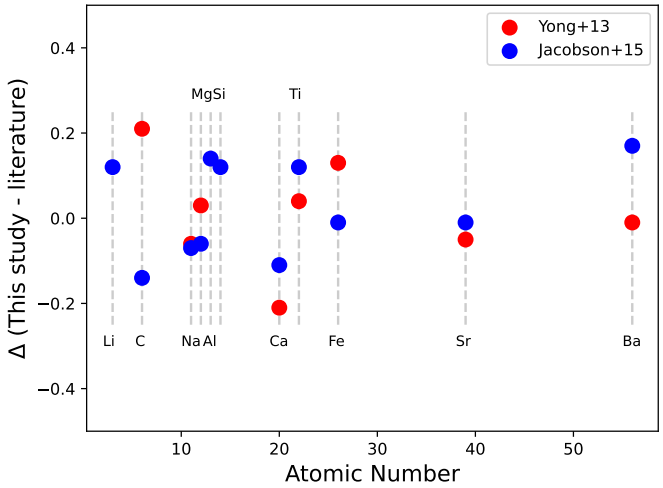

Fig. C.1. Difference of our abundances with respect to those by Yong et al. (2013) and Jacobson et al. (2015), red and blue points respectively, as a function of the atomic number. We consider our LTE abundances but for Li and Na that are provided by Yong et al. (2013) and Jacobson et al. (2015) corrected for NLTE effects.

Appendix D: Contamination of the Na D lines by interstellar features

The photospheric Na D lines at 5889.9 and 5895.9 Å can be contaminated by the same transitions arising from the interstellar medium along the line of sight. We checked that the Na D lines in the spectrum of HE 0057-5959 are not contaminated by interstellar features (see Fig. D.1) because of the large RV of the star. Also the interstellar lines are very weak because of the low colour excess of HE 0057-5959 .

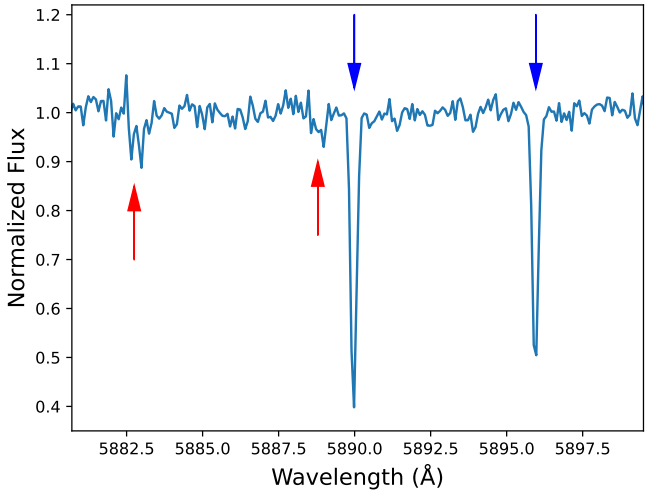

Fig. D.1. Spectral region of the MIKE spectrum of HE 0057-5959 with marked the photospheric and interstellar Na D lines (blue and red arrows, respectively).

Appendix E: Information about the metal-poor Li-rich stars

Tables E.1 and E.2 summarise the main information about the metal-poor Li-rich stars discovered so far in the Milky Way field and in Galactic globular clusters.

Table E.1. Main information about the Li-rich stars discovered so far in the Milky Way field.

Gaia EDR3	ID	$T_{\rm eff}$	log $-g$	[Fe/H]	log($L/L_{\odot}$)	A(Li)$_{\rm NLTE}$	[Na/Fe]	stage	REF
		(K)	(dex)	(dex)	(dex)	(dex)	(dex)		
2918492125161088O	LAMOST J030209.33+135656.3	5118	2.22	–1.74	1.91±0.03	2.10	–0.22	3	1
215823657109094528	LAMOST J055408.54+523559.0	5308	2.51	–2.03	1.69±0.04	2.95	0.75	3	1
673258221256238464	LAMOST J074102.07+213246.6	6189	3.97	–2.33	0.49±0.02	4.05	0.10	1	1
691015471484504704	LAMOST J085208.07+262730.1	5887	3.82	–2.13	0.56±0.05	2.96	0.21	1	1
696658714913856640	SDSS J093627.44+293535.7	5263	3.07	–1.62	1.11±0.20	2.55	—	3	2
883042050539140992	LAMOST J070542.30+255226.6	5287	3.15	–3.19	1.04±0.02	3.01	1.37	3	1
932683488703778048	LAMOST J075816.39+470343.3	5897	4.06	–1.84	0.31±0.09	3.16	0.45	1	1
1005288880051257088	LAMOST J062647.91+603254.0	5962	3.79	–2.29	0.61±0.02	3.16	0.27	1	1
1030551568447702400	GSC 03797-00204	4760	2.16	–2.46	1.84±0.08	2.19	—	4(?)	2
1162478360892154112	2MASS J15221187+0655551	5167	2.40	–2.34	1.75±0.11	2.31	—	3	2
1172619465872571776	SDSS J143207.14+081406.1	4661	2.62	–2.65	1.35±0.45	3.75	—	N/A	2
1181606805198585472	LAMOST J145500.04+125106.2	4830	1.78	–2.68	2.25±0.06	2.15	0.34	4	1
1522817217854702592	LAMOST J131457.78+374110.7	5992	3.94	–2.70	0.46±0.02	3.26	0.68	1	1
1800137243204885120	LAMOST J214610.13+273200.8	5187	2.52	–1.73	1.63±0.11	2.47	0.81	3	1
1918529631627603072	—	4649	1.58	–2.43	2.38±0.07	3.01	0.07	4	3
2604066644687553792	BPS CS22893-010	5374	3.03	–3.12	1.18±0.07	2.68	–0.05	3	4
3199294789168393600	2MASS J04315411-0632100	5662	3.19	–1.85	1.12±0.01	1.86	0.08	N/A	5
3210839729979320064	2MASS J05241392-0336543	4240	1.10	–2.54	2.70±0.06	4.79	1.10	4	6
3360259919923274496	LAMOST J071422.66+160042.5	5116	2.44	–2.16	1.69±0.02	2.21	–0.39	3	1
3665949720385847040	LAMOST J141412.27+001618.7	5033	2.01	–2.56	2.09±0.07	2.32	–0.39	3	1
3687632330203892352	GSC 04958-01069	4580	1.87	–1.54	2.07±0.07	1.88	—	4	2
3926388527100945920	UCAC2 37720962	5196	2.06	–2.23	2.09±0.14	1.99	0.69	3	7
4425538154386975616	2MASS J16070923+0447126	5105	2.56	–1.37	1.56±0.31	2.28	—	3	2
4903905598859396480	HE0057-5959	5420	3.05	–3.98	1.18±0.14	2.09	—	3	8
5441530913278761088	UCAC4 253-045343	4285	1.00	–1.43	2.82±0.07	3.53	–0.27	4	9
5668925276702015872	2MASS J10122548-2030068	4451	1.05	–2.55	2.84±0.36	1.77	—	4	5
6142572036722901504	TYC 7262-250-1	4179	0.92	–1.36	2.85±0.02	4.02	–0.05	4	9
6221353316163376768	UCAC4 308-077592	4086	0.62	–1.86	3.12±0.13	4.25	–0.24	4	9
6298610530751953920	2MASS J14254628-1546301	4287	0.81	–2.08	3.01±0.06	2.96	–0.24	4	5
6381456605897426560	UCAC4 099-098976	5291	2.48	–1.46	1.71±0.01	3.97	–0.24	3	9
6425395014689839744	TYC 9112-00430-1	4394	0.95	–2.21	2.91±0.05	2.27	0.00	4	5
6443920273789215872	2MASS J19524490-6008132	5029	1.79	–1.41	2.30±0.02	1.62	0.14	3(?)	5
6529464133855343872	TYC 8448-00121-1	4731	1.50	–2.45	2.49±0.06	2.71	–0.01	4	5
6668577437377879424	UCAC4 212-183136	4308	1.19	–2.38	2.64±0.07	3.21	+0.58	3	9
6816797308517921792	TYC 6953-00510-1	4836	1.85	–1.93	2.18±0.03	2.25	0.21	4	5

The stars are in order of the *Gaia* EDR3 identification number (we report also the alternative identification number or name used in the literature). Stellar parameters and A(Li)$_{\rm NLTE}$ are those described in Sect. 2. [Fe/H] and [Na/Fe] are those listed in the corresponding papers. The evolutionary stage of each target is obtained as described in Sect. 4: (1) pre-FDU, (2) FDU, (3) post-FDU / pre-RGBb, (4) RGBb. References: (1) Li et al. (2018), (2) Martell & Shetrone (2013) , (3) Sitnova et al. (2023) , (4) Roederer et al. (2014), (5) Ruchti et al. (2011), (6) Kowkabany et al. (2022), (7) Roederer et al. (2008), (8) this study, (9) Susmitha et al. (2024).

Table E.2. Main information about the Li-rich stars discovered so far in Galactic globular clusters. The clusters are in order of right ascension. We list for each target the Gaia ED3 identification number and the alternative identification number or name used in the literature. Stellar parameters and $A(Li)_{NLTE}$ are those described in Sect. 2. [Fe/H] and [Na/Fe] are those listed in the corresponding papers. The evolutionary stage of each target is obtained as described in Sect. 4: (1) pre-FDU, (2) FDU, (3) post-FDU / pre-RGBb, (4) RGBb. References: (1) Smith et al. (1999), (2) D'Orazi et al. (2015), (3) Sanna et al. (2020), (4) Aguilera-Gómez et al. (2022), (5) Ruchti et al. (2011), (6) Kirby et al. (2016), (7) Mucciarelli et al. (2019), (8) Kraft et al. (1999), (9) Monaco et al. (2012), (10) Koch et al. (2011), (11) Gruyters et al. (2016).

CLUSTER	Gaia EDR3	ID	T_{eff}	$\log -g$	[Fe/H]	$\log(L/L_{\odot})$	$A(Li)_{NLTE}$	[Na/Fe]	stage	REF
			(K)	(dex)	(dex)	(dex)	(dex)	(dex)		
N362	4690838559145577728	V2	3651	0.33	-1.26	3.21	0.41	–0.38	4	1
N362	4690838726645395840	15370	5004	2.27	-1.26	1.82	2.44	—	3	2
N1261	4733703810220702976	GES J03115070-5514001	4984	2.31	-1.27	1.78	3.16	—	3	3
N3201	5413582186704791168	97812	5001	2.44	-1.59	1.65	1.55	—	3	4
M68	3496374958317915648	Stet-M68-S232	4488	0.99	-2.23	2.91	2.56	0.14	4	5,6
M68	3496399735985613312	Stet-M68-S534	5397	3.16	-2.23	1.06	2.35	—	3	6
N5053	3938494188778278272	N5053-S79	5277	2.71	-2.27	1.47	2.59	—	3	6
OCen	6083508196239683968	25664	5061	2.46	-1.80	1.65	1.83	0.87	3	7
OCen	6083703428274945280	126107	5059	2.40	-1.80	1.71	1.71	0.14	3	7
M3	1454783694639968384	M3-IV101	4283	0.93	-1.50	2.89	2.99	0.34	4	5,8
N5897	6252666548333610624	Tes01-WF4-703	4804	1.76	-1.90	2.26	1.34	—	4	6
M4	6045462826174755328	37934	5914	4.13	-1.16	0.25	2.71	0.18	2	9
N6397	5921744197274599040	6282	6241	4.12	-2.02	0.36	4.07	—	2	10
M30	6816582040462535552	132	5598	3.54	-2.27	0.74	2.61	—	1	6,11
M30	6816574859276974336	7229	5409	3.25	-2.27	0.98	2.78	—	3	6